On the spatial-temporal development of turbulent spots on a serrated trailing edge

A. Juknevicius,[1] and T. P. Chong[2]
School of Engineering and Design, Brunel University London, Uxbridge, UB8 3PH

Aim of the paper is to investigate the flow in the close vicinity of flat-plate insert-type trailing edge serrations. It is now firmly established that aerofoil subjected to a serrated trailing edge is quiet. Recent advances in the analytical and numerical solutions have established several mechanisms that can help to explain the causes of the lower level of self-noise radiation by a serrated aerofoil. Some high fidelity experimental works, such as the time-resolved Particle Image Velocimetry (PIV), have been used recently to track the evolution of a fully-developed turbulent boundary layer flow structures over a serrated trailing edge. However, due to the high cost and technical challenging, the time-resolved PIV measurements still have some limitations in the construction of a complete spatial and temporal evolution of these small-scale turbulent structures. The current work seeks to develop a simple technique by artificially generating the turbulent spots – the so called "building block" of the turbulent boundary layer, and to track in the space and time domains a complete evolution of these spots over the serrated trailing edge of an aerofoil using the ensemble-averaging analysis method for the hot-wire data. The test was conducted on a symmetrical NACA0008 aerofoil under zero-lift conditions and at a Reynolds number 1.12×10^5. Aero-acoustic measurements at these conditions confirm that significant broadband self-noise reduction can be achieved by a serrated trailing edge. After gathering the relevant boundary layer data, a preliminary examination of the velocity perturbation and turbulence intensity distributions near the straight trailing edge would confirm the classical turbulent spot structure that can typically be found in the literature. However, in the case of a serrated trailing edge, it is observed that each passage of a turbulent spot, especially at its so called 'calm region', would draw high momentum flow (i.e. positive velocity perturbation) *periodically* from the sawtooth gap towards the sawtooth surface. It is believed that this periodic calming and stabilization effect of the boundary layer might represent the general mechanism for the reduction of the self-noise generated at the trailing edge, although currently more data analysis is still underway to dissect the internal flow details of the turbulent spot at the serrated trailing edge.

Nomenclature

C	=	aerofoil chord length
b	=	aerofoil span
f_{sg}	=	spot generation frequency
Re	=	Renolds number
U_∞	=	freestream velocity
λ	=	serration wavelength
$2h$	=	serration amplitude
t_p	=	pulsewidth
γ	=	turbulence intermittency factor
α	=	effective angle of attack
α_g	=	geometric angle of attack

[1] PhD Student, Department of Mechanical and Aerospace Engineering, auris.juknevicius@brunel.ac.uk, Non-AIAA member.
[2] Senior lecturer, Department of Mechanical and Aerospace Engineering, t.p.chong@brunel.ac.uk, Member AIAA.

I. Introduction

Wind energy industry experts are drawing a clear picture for the future of the alternative energy source and are increasingly emphasising its significance as part of the energy infrastructure. A publication by Wind Europe has outlined several scenarios for future development of wind energy in Europe. The *Central scenario* estimates 323GW of wind energy capacity installed until 2030, 253GW (or 78%) coming from onshore wind turbines and 70GW (or 22%) from offshore [1]. A more than double increase compared to the recorded capacity of 160GW at the end of 2016 signifies the role of wind energy in terms of future energy production in Europe. An expected 78% of the wind energy coming from onshore wind farms implies that the prominent issue of wind turbine noise, that might complicate a more widespread production of wind power on land, will maintain its relevance for at least the next 15 years due to the aforementioned future increase in wind energy capacity that is likely to require wind turbine installations in close proximity to communities. This fortifies the validity of and need for research targeting all possible methods of wind turbine noise reduction.

When considering the sources of wind turbine noise, the major contribution is attributed to the aerodynamic noise generated by the blades. More specifically, it is the turbulent boundary layer – trailing edge (TBL-TE) interaction noise, as described in [2], that is regarded as the dominant aerodynamic noise source [3]. The noise issue has been targeted by different passive flow control methods such as poro-serrated or brushed trailing edges, however saw-tooth shaped trailing edge serrations have so far attracted the most extensive research due to their relative technological simplicity. Therefore, the performance aspect of trailing edge broadband noise reduction by saw-tooth serrations is well established in [3]–[9] and a number of other studies. Nevertheless, a consensus with regards to the exact mechanism of trailing edge noise reduction by trailing edge serrations is yet to be reached.

A study presented in [10] has partly focused on the steady and unsteady aerodynamics around an aerofoil to provide more insight into the mechanism of trailing edge noise reduction by serrations. Six flat plate trailing edge serration configurations with varying serration lengths and wavelengths have been tested on a NACA6512-10 cambered aerofoil placed in an open-jet wind tunnel at 5° angle of attack. The study has observed that mean velocity profiles of the boundary layer along the span of the root of a single serration sawtooth have shown only minor differences in comparison to the profiles measured at the corresponding locations on a straight trailing edge, indicating that serrations only have a minor or no effect on the boundary layer upstream of serrations. Similarly, turbulent velocity profiles in the boundary layer for baseline and serrated cases tend to become more comparable as the measurement position shifts closer to the serration root, although a 30% increase in maximum turbulence intensity is observed in the serration case, even at the serration root. At the serration tip, however, mean velocity profile is 15% thicker when compared to the baseline case and for this reason turbulent velocity profiles indicate turbulence being shifted away from the surface.

Part of an experimental study by [11] has used a liquid crystal technique to visualise the effects of turbulent flow passing through a serrated trailing edge on a flat plate. Pre-heated surface allows crystals to change colour in relation to an increase or a decrease in heat transfer that can be related to the different flow regime. The study identifies higher time-averaged heat transfer rates at the side edges and tips of serrations, implying that this must be induced by a stronger flow regime than a turbulent boundary layer. This strongly correlates to surface pressure fluctuation measurements, where higher wall pressure spectral energy levels have been located near the serration edges and tips. The authors relate these observations to the presence of convective pressure-driven vortical structures forming at the serration edges (and convecting into the tip region) that are a potential contributor to broadband noise reduction. [12] has used a similar experimental approach of surface-pressure fluctuation measurement and have shown that broadband noise reduction is due to the major reduction in phase speed of turbulence convection near saw-tooth edges as well as the reduction in coherence of pressure measurements along serration edge.

Strong support towards the observations described in the previous paragraph is provided by a study in [13]. Time-resolved tomographic particle image velocimetry PIV has been used to study the three-dimensional flow field on the suction side of a NACA0018 aerofoil with trailing edge serrations, placed in an open-jet wind tunnel with a geometric angle of attack of 4°. Straight and serrated trailing edge cases have shown strong similarities in terms of mean velocity and turbulent fluctuation boundary layer profiles, indicating that the turbulent boundary layer upstream of serrations is only weakly affected by their presence and that is in agreement with [10]. Downstream of serrations the flow becomes complex with streamwise-oriented vortical structures forming around serration edges and additional counter-rotating flow structures are present in the serration gaps. These structures are believed to induce secondary effects, such as the funnelling of the incoming flow that changes the serration effective angle (φ') as reported by [11], that could contribute to the the way broadband noise is scattered. This effect is also evident from the contours of time averaged u (streamwise) velocity component at the serration surface that show the flow approaching the serrations seeping into the serration gaps. This observation has later been verified by a numerical study in [14], where in case of a serrated NACA0018 aerofoil under zero lift conditions, the near-wall ($y=0.5mm$ from the wall) spatial distribution

of time averaged mean velocity *u* (streamwise) component has shown an increase moving away from the root towards the tip, indicating an acceleration of the flow.

The present work aims to investigate the evolution of the three-dimensional flow structure through the use of hot-wire anemometry. This is achieved by employing a technique allowing the 'recreation' of a process of random formation of turbulent spots that occurs in the final stages of natural flow transition from laminar to turbulent. These 'spots', intermittently appearing within an instable laminar boundary layer, begin merging (turbulence intermittency factor γ, refer to [15], of $0 < \gamma < 1$) and eventually coalesce into a fully turbulent boundary layer ($\gamma = 1$). The technique relies on artificial generation of 'packets' of turbulence, known as turbulent spots, that convect over an aerofoil from their origin and eventually travel past the trailing edge into the aerfoil wake. Strong similarities between naturally occurring and artificially generated turbulent spots are outlined in [16] and [17], hence validating the use of the proposed experimental technique as a tool to study the interaction of turbulent flow/pressure fluctuations with the aerofoil trailing edge. Further validation is provided in [18], [19] and [20] that have identified a number of similarities between a turbulent spot and turbulent boundary layer in terms of their structure and the mechanisms of growth. Therefore, for the purpose of the present study, a single turbulent spot is assumed to be an isolated part of and represent a turbulent boundary layer that is normally induced under experimental conditions by introducing a tripping element to the flow. Hence, instead of measuring the mean properties of a fully established turbulent flow, its evolution as it passes through the measurement volume can be demonstrated. Sections B and C will outline the detailed methodology to clarify how this is achieved experimentally.

II. Experimental Setup and Data Analysis Techniques

A. Wind tunnel facilities and instrumentation

1. Aero-acoustic wind tunnel facility

Aero-acoustic noise measurement experiments have been carried out in the aero-acoustic research facility in Brunel University London, described in greater detail in [21]. Airflow is provided by a low freestream turbulence intensity (TU = 0.1 % - 0.2%) aero-acoustic wind tunnel having dimensions of 0.1 m x 0.3 m at the rectangular nozzle exit.

Far field noise measurements are conducted using an 8 condenser microphone polar array located at 1 m from the mid-span of the trailing edge with microphones placed at polar angles of -45° to 45°. Velocities under investigation range from 12 ms^{-1} to 30 ms^{-1}, corresponding to Reynolds numbers based on *C* of 1.2 x 10^5 and 3 x 10^5 respectively. Aerofoil is placed at a 0° angle of attack unless specified otherwise. Note that due to potential jet deflection as a result of the wind tunnel boing open jet, a 0° effective angle of attack α_e (or zero pressure gradient) has been established by measuring the streamwise distribution of static pressure along the aerofoil chord. Flow transition is induced by introducing a zig-zag shaped tripping element (t = 0.6 mm) at x/C = 0.17 from the leading edge on both upper and lower sides of the aerofoil. Data were sampled for 20s at 40kHz sampling frequency by a 24-bit analog-digital card from National Instruments. The data is windowed and the Power Spectral Density (PSD) of 1Hz bandwidth is computed from a 1024 point FFT.

2. Aerodynamic wind tunnel facility

Aerodynamic measurements were conducted in a low freestream turbulence intensity TU = 0.3 % - 0.4 % closed section, open circuit wind tunnel in the aerodynamics laboratory, Brunel University London. The wind tunnel of 0.5 m x 0.5 m cross-section is paired with a three-dimensional traverse system (having a motion resolution of ±0.01 mm in all three axes) to facilitate flow measurements in a selected three-dimensional flow domain. The aerofoil is mounted inside the wind tunnel at a 0° angle of attack unless specified otherwise. Therefore, the known effects of streamwise pressure gradient on turbulent spot development [22] are only due to the inherent pressure gradient of the aerofoil. Data are collected at a freestream velocity of U_∞ = 8.5 ms^{-1}, corresponding to Reynolds number of 1.12 x 10^5 based on chord.

B. Design of NACA0008 aerofoil and turbulent spot generation technique

The aerofoil under investigation is a NACA 0008 symmetrical profile with 0.2 m chord and 0.5 m span and is demonstrated in Fig. 1. This aerofoil has been selected mainly due to its lower thickness and less severe adverse pressure gradient that is favourable for the proposed experimental technique. Aerofoil is designed such that the trailing edge, between x/C = 0.8, and x/C = 1, can be detached from the main body, between the leading edge and x/C = 0.8, and interchanged between a straight trailing edge (baseline case) and a slotted trailing edge used to accommodate the flat plate insert-on type serrations.

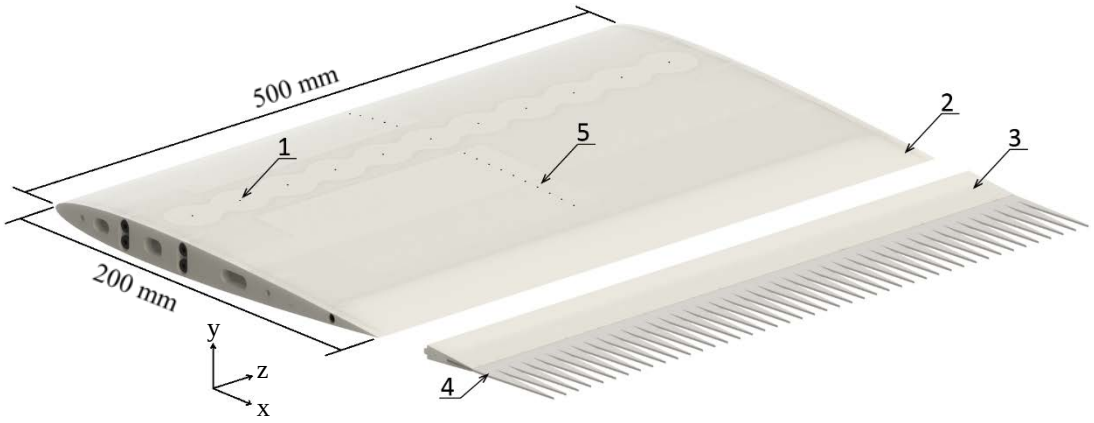

Fig. 1 NACA 0008 aerofoil and main features: 1) 0.5 mm diameter orifice, 2) Straight trailing edge, 3) Slotted trailing edge, 4) $\lambda_{6.67}h_{26.67}$ serrations and 5) 0.5 mm diameter static pressure taps; and adopted coordinate system

Serration design has been selected after a series of broadband trailing edge noise measurements conducted in the aero-acoustic wind tunnel facility described earlier. A total of 9 serration designs, varying in serration amplitude, *2h*, and serration wavelength, *λ*, have been tested. The results, that will be discussed in later paragraphs, have identified serrations $\lambda_{6.67}h_{26.67}$ to be the most suited for the current study. Due to the serration being laser cut, they have amplitude 2h of 25mm and wavelength λ of 6.7mm.

Serrations are applied to the trailing edge such that they extend from the baseline trailing edge, in turn increasing the effective chord length of the aerofoil by the length of the amplitude (2h) of the serrations, see Fig. 2, when compared to the baseline aerofoil. Serration root therefore coincides with the trailing edge of the baseline case.

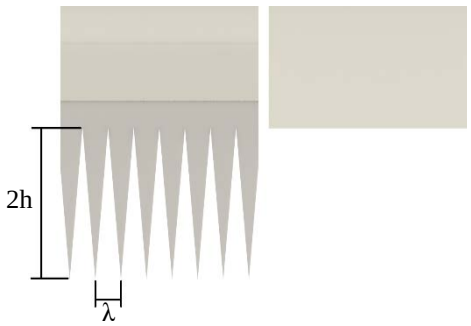

Fig. 2 Serrated trailing edge, left, and baseline trailing edge, right; 2h - serration amplitude, λ – serration wavelength

As mentioned earlier, the experimental technique used in this experiment relies on artificially generating turbulent spots that are then measured to allow the reconstruction of their spatial-temporal development as they travel past the flow domain of interest. Spots were triggered by injection of air jets at x/C = 0.3 downstream of the leading edge into the laminar flow, hence inducing localised disturbances. Jets are generated by miniature speakers driven by a 16Hz pulse waveform signal which was also used as a reference signal for subsequent ensemble averaging of the flow velocity data. Growth of the disturbances into turbulent spots by natural amplification is achieved using a 1.7 millisecond duration low magnitude jet, although this parameter was found to be highly dependant on the overall experimental setup.

To more accurately reproduce the conditions under which TBL-TE interaction noise occurs, turbulent spots are generated on both upper and lower sides of the aerofoil. This has proven to be a delicate procedure, hence, before carrying out the experiment, it was established that the spots generated on the two sides of the aerofoil are comparable in terms of their features, size, magnitude as well as time of arrival (time it takes for the spot to arrive from its origin to the measurement point) when measured at a given distance downstream of the spot origin.

Once generated, the spot then convects downstream, eventually passing the trailing edge and the flow domain at which the measurements are taken. Providing that the signal of velocity fluctuations induced by the spot's passage can be distinguished from the signal of an *otherwise laminar flow*, velocity fluctuation signature of each individual turbulent spot can be measured using hot-wire anemometry. Therefore, the necessary condition of laminar flow covering the full aerofoil chord is ensured by reducing surface roughness as well as surface features that have the potential to induce transition.

C. Data processing methods

Experimental work is carried out by collecting velocity fluctuation data at selected measurement points. With the current experimental methodology, measurements are taken at selected X-Z and Y-Z planes (refer to Fig. 1 for the coordinate system). All measurements are taken from a common reference point used in both baseline and serrated trailing edge cases, although the dimensions of the measurement domains are different. The reference point is located 9 mm upstream of the trailing edge as demonstrated in Fig. 3.

In terms of measurements in the X-Z plane, domains of 16 mm x 7.4 mm and 35 mm x 7.4 mm are covered for baseline and serrated cases respectively and the number of domain points for both cases is summarized in Table 1. Single wire measurements of u velocity component in this plane are taken at 4 distances from the aerofoil surface: 0.4 mm, 1 mm, 1.6 mm and 2.9 mm, as demonstrated in Fig. 5.

Table 1 Summary of single wire measurement grid in X-Z plane

	Baseline, $\lambda_0 h_0$	Serrated, $\lambda_{6.67} h_{26.67}$
# of points across Z	13	13
# of points across X	17	36
Total # of points across the plane	221	468

In terms of measurements in the Y-Z plane, each plane covers an area of 7.4 mm x 6.1mm for both baseline and serrated trailing edge cases. The number of measurement points and measurement planes with their locations for both cases is summarized in Table 2. Single wire measurements of u velocity component in this plane are limited to the upper side of the aerofoil as shown in. However, cross-wire measurements have been taken to collect data of u (streamwise) and w (spanwise) velocity components in the wake region, covering the flow coming from both upper and lower sides of the aerofoil. The number of measurement points and measurement planes with their locations is summarized in Table 3. For clarification, Fig. 3 illustrates the orientation of the described measurement planes with respect to the aerofoil trailing edge.

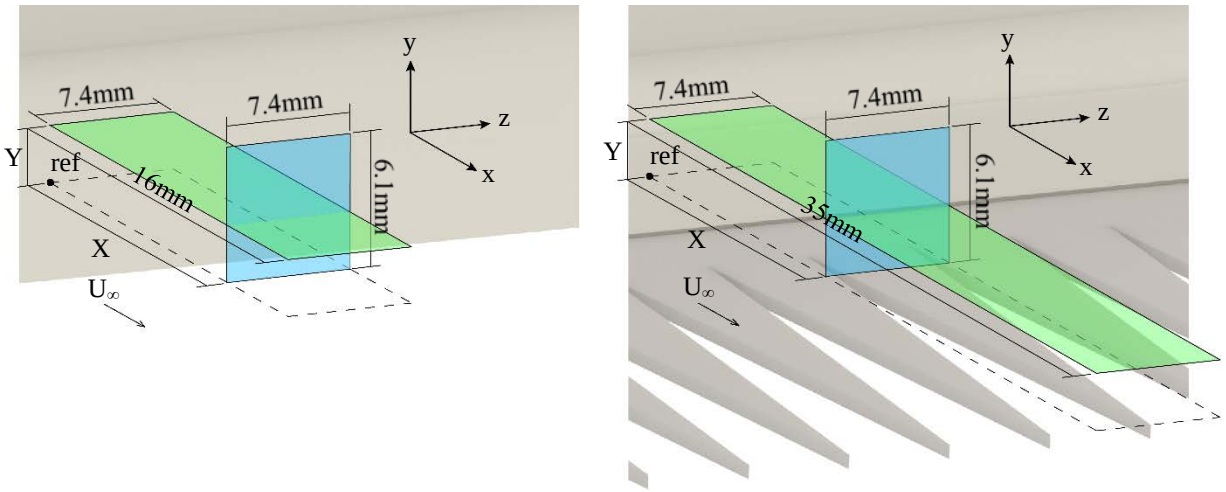

Fig. 3 Illustration of X-Z (green) and Y-Z (blue) measurement planes on a baseline (left) and serrated (right) trailing edges; 'ref' indicates the common point of reference for the two trailing edges

Table 2 Summary of single wire measurement grid in Y-Z plane

	Baseline, $\lambda_0 h_0$	Serrated, $\lambda_{6.67} h_{26.67}$
# of points across Z	13	13
# of points across Y	30	30
Total # of points across the plane	390	390
Locations of planes measured (in terms of distances from the reference point, mm)	0, 7, 16	0, 7, 11, 19, 29, 33

Table 3 Sumary of cross-wire measurement grid in Y-Z plane

	Baseline, $\lambda_0 h_0$	Serrated, $\lambda_{6.67} h_{26.67}$
# of points across Z	13	13
# of points across Y	57	57
Total # of points across the plane	741	741
Locations of planes measured (in terms of distances from the trailing edge, mm)	1, 7	1, 7

The streamwise velocity component *u* was measured using a DANTEC 55P14 single hot-wire probe operated at an overheat ratio of 1.8 with constant-temperature anemometer. Hot-wire signals are sampled at a frequency of 5kHz after passing through a low-pass filter and digitised by a 12-bit A/D card. A typical data set for a single measurement point contains 130,000 samples covering a sequence of approximately 400 individual turbulent spots.

Two component velocity signals u and w are measured in the aerofoil wake region using a DANTEC 55P64 X-wire probe. Parameters for data acquisition as well as the overheat ratio are identical to those described in the previous paragraph. Velocity and yaw calibrations were carried out in the free stream. For velocity calibration, a fourth-order polynomial from the best fit of the calibration data was used. For the yaw calibration, the X-wire has been rotated from -45° to 45° at 5° increments. Temperature corrections are applied to both single and cross wire measurements.

The acquired signal of velocity fluctuations induced by the passage of turbulent spots is used to generate an ensemble of turbulent spots (see Fig. 4a), using the rising edge of the triggering pulse as a reference. It is then averaged to obtain a mean velocity signature for every measurement point. Fig. 4b illustrates typical mean velocity signatures at a number of distances y measured across approximately one boundary layer thickness.

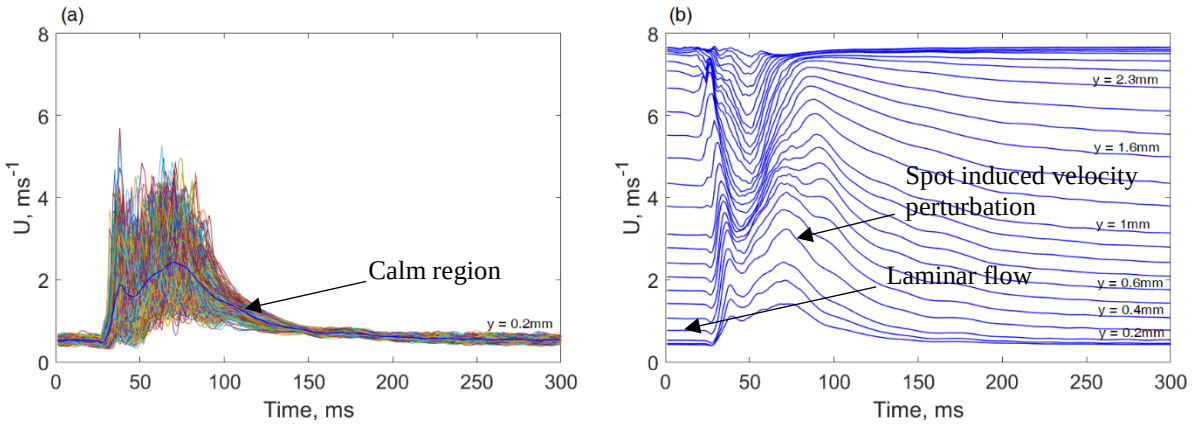

Fig. 4 An ensemble of 400 turbulent spot velocity signals (coloured lines) and an ensemble averaged velocity signature (blue) at y=0.2 mm on the left; ensemble averaged velocity signatures at different locations across one boundary layer thickness on the right

The obtained mean velocity is then used to calculate velocity perturbations and RMS velocity fluctuations induced by the spot's passage. If temporal variation of ensemble-averaged velocity *u* at each of the measurement points is denoted by $\langle u(x,y,t)\rangle$, velocity perturbation ũ induced by an ensemble-averaged turbulent spot in relation to an undisturbed laminar boundary layer (Fig. 4b) is expressed as:

$$\tilde{u}(x,y,t) = \frac{\langle u(x,y,z,t)\rangle - u_L(x,y,z)}{u_\infty(x)}$$

where $u_L(x,y,z)$ is the local velocity of an undisturbed laminar boundary layer and $u_\infty(x)$ is the velocity of the freestream flow.

Similarly, the temporal variation of ensemble-averaged rms fluctuations of u at each measurement point can be determined by

$$u'(x,y,t) = \sqrt{\frac{\sum_{i=1}^{N}[U(x,y,z,t) - \langle U(x,y,z,t)\rangle]^2}{N}}$$

where *u(x,y,z,t)* is the temporal variation of u of each individual spot and N is the number of spots in the ensemble. The same equations and procedure are also applied to the data of spanwise velocity component *w*.

From the obtained data, each measurement point is represented by a contour plot (see Fig. 5) of velocity perturbations ũ (normalised by the freestream velocity) in time domain. The perturbation contours can be interpreted as the change of momentum relative to the local laminar value – a momentum increase (red or yellow) or a decrease (blue). The same principle is used to present the rms velocity fluctuations u', that can be interpreted as a change in turbulence intensity relative to the local laminar boundary layer.

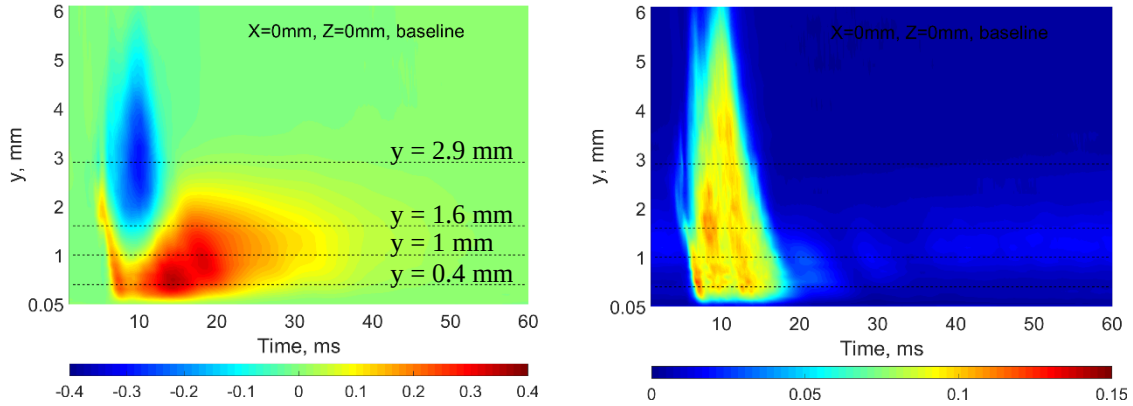

Fig. 5 Typical contour plots of velocity perturbations $\widetilde{U}$ (left) and rms velocity fluctuations u' (right) caused by an ensemble-averaged turbulent spot

III. Experimental results and discussion

A. Aeroacoustic noise measurements

Prior to commencing the intended and previously described hydrodynamic study, it was first necessary to establish noise reduction capability of the flat plate insert-on type serrations applied to the current aerofoil configuration. Any observed noise reductions would imply that the presence of trailing edge serrations introduces changes to the hydrodynamic behavior of the flow in the vicinity of trailing edge serrations, hence validating the selected experimental approach to this study.

Fig. 6 displays the contours of difference in sound pressure level (SPL) between the baseline aerofoil ($\lambda_0 h_0$) with straight trailing edge and the nine trailing edges ($\lambda_{3.33}h_{13.33}$, $\lambda_{3.33}h_{26.67}$, $\lambda_{3.33}h_{40}$, $\lambda_{6.67}h_{13.33}$, $\lambda_{6.67}h_{26.67}$, $\lambda_{6.67}h_{40}$, $\lambda_{13.33}h_{13.33}$, $\lambda_{13.33}h_{26.67}$ and $\lambda_{13.33}h_{40}$) for velocities ranging from 12 ms^{-1} to 30 ms^{-1}. A positive ΔSPL therefore represents a noise reduction and negative ΔSPL represents a noise increase. Note that due to low background noise of the wind tunnel, the aerofoil with the quietest trailing edge is still capable of radiating higher noise levels than the background.

The results clearly demonstrate that all nine serration models added to the baseline aerofoil have a significant effect on the radiated noise. As expected, noise reduction performance tends to increase with increasing serration amplitude h as well as increasing serration wavelength λ although, as already demonstrated by earlier studies, the former has a more substantial effect and this is reflected in the results.

With the exception of serrations $\lambda_{13.33}h_{13.33}$, all the others appear to follow a similar trend where noise reductions of up to 6dB are observed across the whole velocity range. Comparing Fig. 6e through Fig. 6i, only minor differences, mainly in the lower frequency and lower velocity regions, can be observed. Considering that the difference in noise performance between serrations $\lambda_{6.67}h_{26.67}$ and the best performing $\lambda_{3.33}h_{40}$ is insignificant, the former has been selected for further study. The main reason for that is the serration physical dimensions that are significantly smaller in comparison to $\lambda_{3.33}h_{40}$. Considering that the flow domain covering at least one full serration needs to be measured, reducing its size allows achieving a similar experimental outcome with significantly less experimental time required.

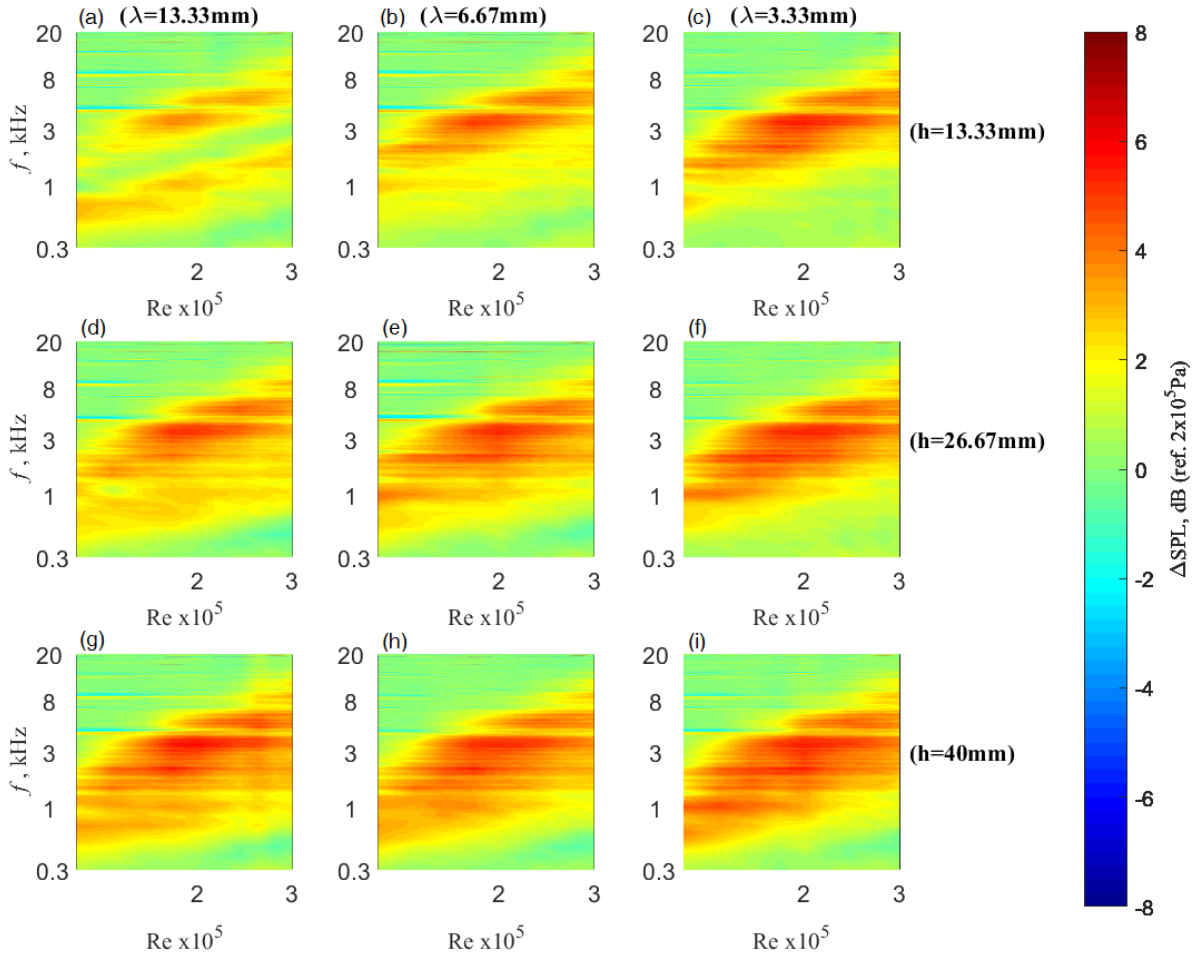

Fig. 6 Contours of ΔSPL, dB produced by $\lambda_{13.33}h_{13.33}$, (b) $\lambda_{6.67}h_{13.33}$, (c) $\lambda_{3.33}h_{13.33}$, (d) $\lambda_{13.33}h_{26.67}$, (e) $\lambda_{6.67}h_{26.67}$, (f) $\lambda_{3.33}h_{26.67}$, (g) $\lambda_{13.33}h_{40}$, (h) $\lambda_{6.67}h_{40}$ and (i) $\lambda_{3.33}h_{40}$ flat plate insert-type serrated trailing edges; microphone polar angle θ = 90°

B. Aerodynamic flow measurements

1. Turbulent spot and the 'calm region'

The results presented in the aerodynamic flow measurement section in large part will focus on the effect that the trailing edge serrations have on the so called *calm region* of the turbulent spot. It is generally observed that this region undergoes the most significant serration induced changes and this will be described in greater detail in the following paragraphs.

Fig. 7 demonstrates a side by side comparison of ensemble-averaged turbulent spots measured at the same location (streamwise plane of symmetry of the spot, 131mm downstream of its origin) for the baseline and serrated trailing edge cases. As mentioned earlier, it was necessary to ensure the similarity of the spots generated in the two trailing edge cases. Initial observation of the plots reveals that both velocity perturbation and rms velocity fluctuation contours appear to be nearly identical in terms of both their shape and magnitude across the whole spot. This validates any comparisons made between the baseline and serrated case results in the following paragraphs.

Closer inspection of the velocity perturbation contours in Fig. 7 shows that the turbulent spots exhibit typical features such as the leading edge overhang (region I), the negative perturbation region (region II), the positive perturbation region (region III) as well as the calm region (region IV).

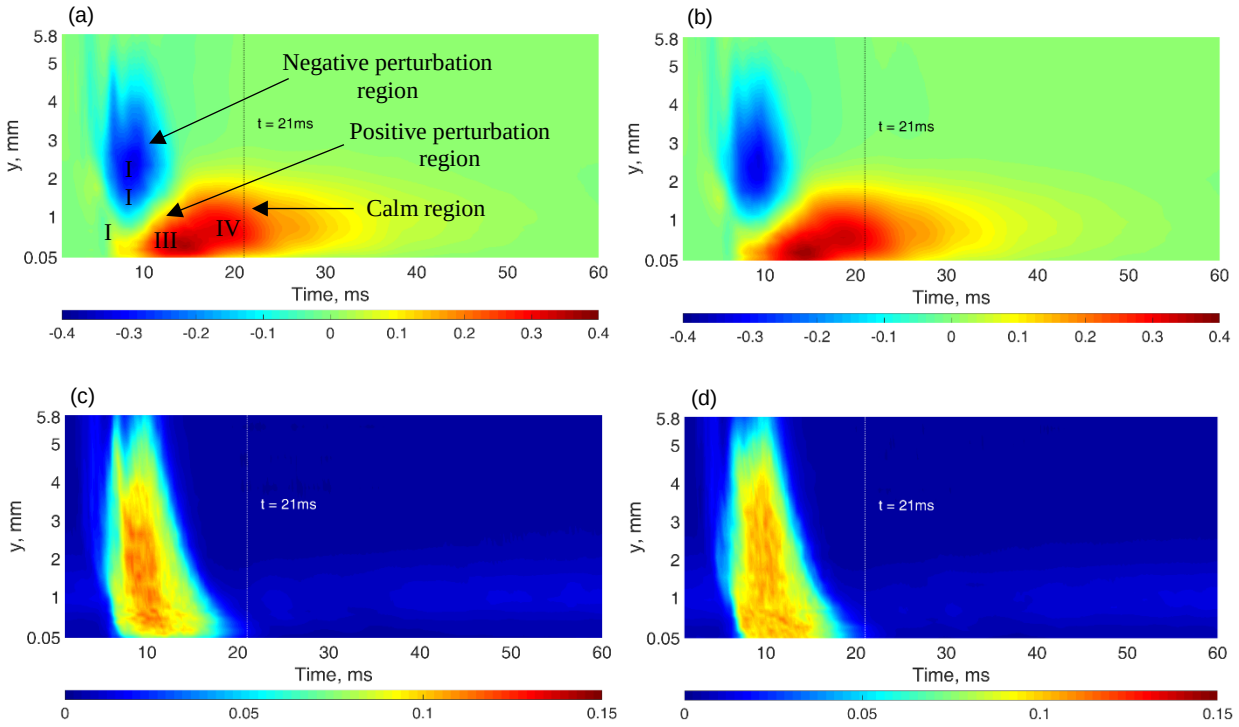

Fig. 7 Ensemble-averaged turbulent spot velocity perturbation profiles measured on the baseline (a) and serrated (b) trailing edges; and rms velocity fluctuation profiles measured in the baseline (c) and serrated (d) trailing edges; dashed line indicates the time at which the profile is plotted

Region IV, or the 'calm region' of the turbulent spot, is known to posess high stability as a result of high momentum which tends to stabilise the flow in that region. The stability is illustrated by comparing boundary layer velocity profiles measured in the local laminar flow and at a selected location within the calm region and this is shown in Fig. *8*. As expected, boundary layer profile measured within the spot is significantly fuller than the laminar profile. This implies that in order for the calm region to be destabilised, it must interact with a strong flow regime and this will be discussed in the following paragraphs.

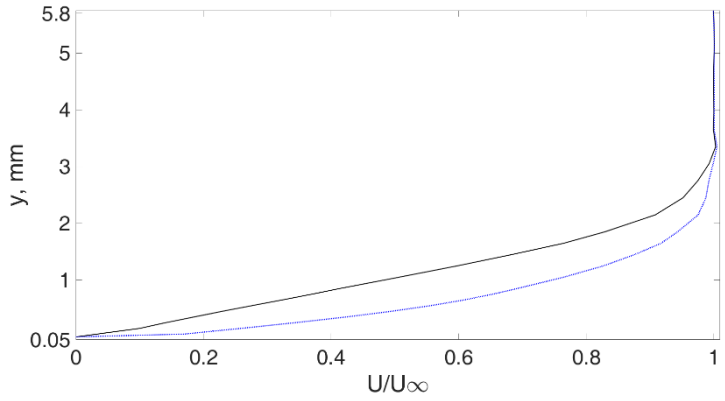

Fig. 8 Local laminar boundary layer profile (black solid line) and boundary layer profile measured within the calm region of the spot (blue line) at t = 17 ms, as demonstrated in Fig. 7

2. Turbulent spot in y-z plane

Results presented in Fig. 9 demonstrate velocity perturbation contours caused by the passage of an ensemble averaged turbulent spot through a y-z measurement plane located just prior to entering the wake region (for the baseline trailing edge case) or entering the serration region (for the serrated trailing edge case). Direction of the freestream flow and orientation of the measurement plane are as indicated in Fig. 3.

Fig. 9a indicates the first instance of spot arrival at t = 5.6ms, where we can see two regions of low magnitude positive perturbations caused by the leading edge overhang and low magnitude negative perturbation indicating the location of the negative perturbation region. At t = 7.2ms, the overhang has already passed and the negative perturbation region increases, until it eventually grows to its full extent at t = 9ms. Similarly, a positive perturbation region of larger extent appears near the wall. As expected, serrated trailing edge results demonstrate comparable structures, again suggesting the similarity of turbulent spots generated in the two trailing edge cases.

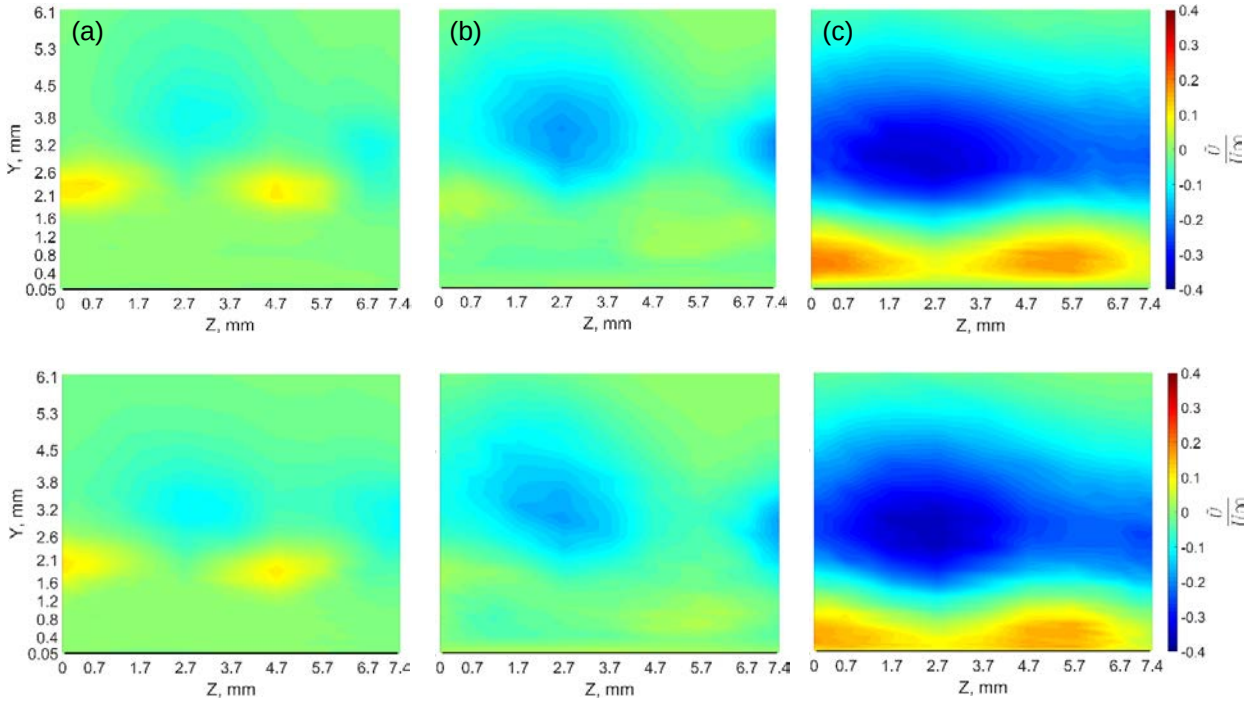

Fig. 9 Velocity perturbation contours in y-z plane on the baseline (top row) and serrated (bottom row) trailing edges at (a) t = 5.6 ms, (b) t = 7.2 ms and (c) t = 9 ms; measured at 2 mm upstream of the trailing edge (for the baseline case) or the serration root (for the serrated trailing edge case)

The similarity is further emphasised in Fig. 10. Contours at t = 12.6ms demonstrate that the calm region expands and now covers the full span of the plane, also with much larger extent and magnitude. As the spot passes, the negative perturbation region dissipates and magnitude of positive velocity perturbations within the calm region reduces as shown in Fig. 10b. It continues to reduce gradually and at t = 36.4ms only the trailing edge of the calm region is visible.

Several conculsions can be drawn from the presented results:

1. During the complete passage of an ensemble averaged turbulent spot, both baseline and serrrated trailing edge cases display nearly identical structures at every presented time instance and this also holds true for the measurements taken at a more upstream measurement plane. This suggests an important implication that any indication of change in the turbulent spot structure in any of the downstream measurement planes that coincide with the serration region must be *induced by the presence of trailing edge serrations.*
2. Strong similarity in the development of the turbulent spot in the two cases shows that the presence of serrations has virtually no effect on the near upstream flow. This goes in line with the observation made in [10] has shown similar boundary layer velocity profiles when measured across one serration saw-tooth and the corresponding locations on a baseline trailing edge.

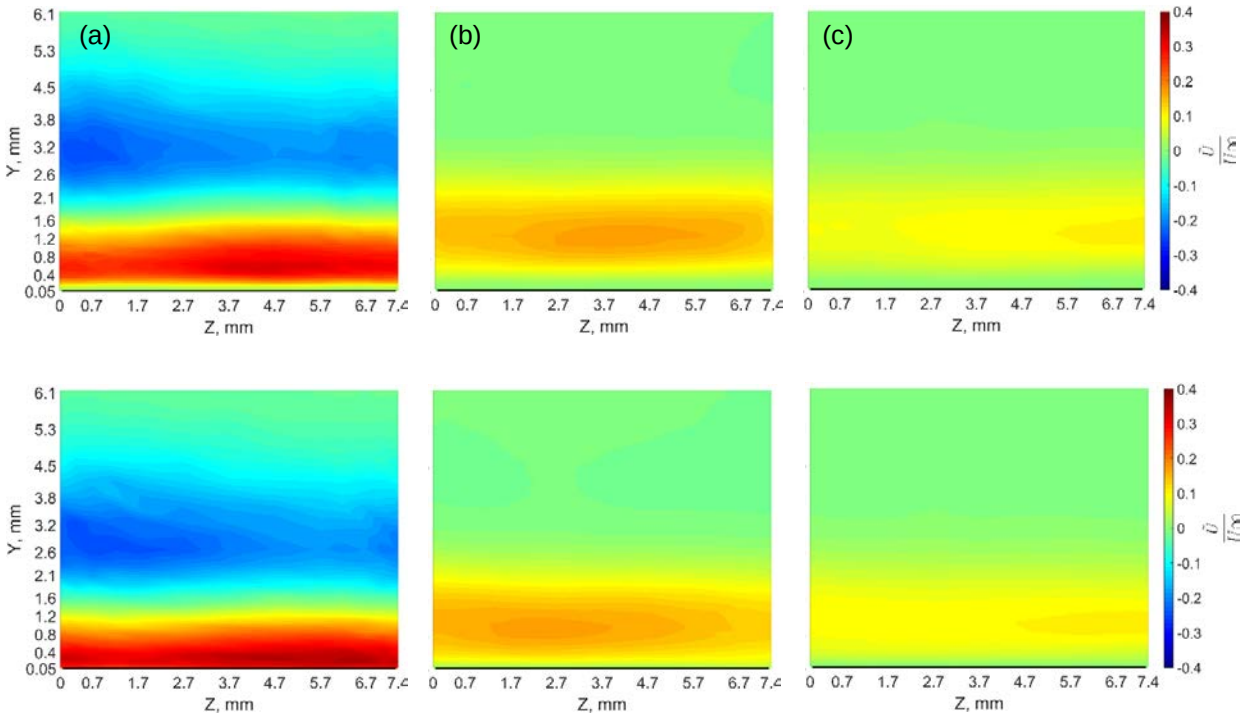

Fig. 10 Velocity perturbation contours in y-z plane on the baseline (top row) and serrated (bottom row) trailing edges at (a) t = 12.6 ms, (b) t = 30 ms and (c) t = 36.4 ms; measured at 2 mm upstream of the trailing edge (for the baseline case) or the serration root (for the serrated trailing edge case)

Previous section has presented the results of measurements taken upstream of the serration region and no significant differences have been indicated. Noticeable changes to the flow structure, however, can be identified by analysing any of the downstream measurement planes. Hence, the Z-Y plane being presented is measured at $x_s/2h$ = 0.8, where x_s is the streamwise distance from the serration root to the measurement plane. This plane is selected as it is the most representative of the flow phenomenon that is seen to occur. Generally, other measurement planes have followed a similar pattern, although have displayed different magnitudes – lower magnitudes in the region closer to the serration root and higher near the tip.

Fig. 11a demonstrates the flow prior to the spot's arrival, therefore virtually no traces of perturbations are seen. However, rms velocity fluctuation plots are demonstrating significant levels of turbulence intensity in the serration root regions. This implies that at freestream flow conditions, serration roots are inducing a strong flow regime that causes significant streamwise fluctuations to appear. However, as the spot approaches (t = 11.6ms), high intensity regions begin to be disrupted. The effect becomes even more significant at t = 19ms, where indication of the arrival of the turbulent spot calm region is evident.

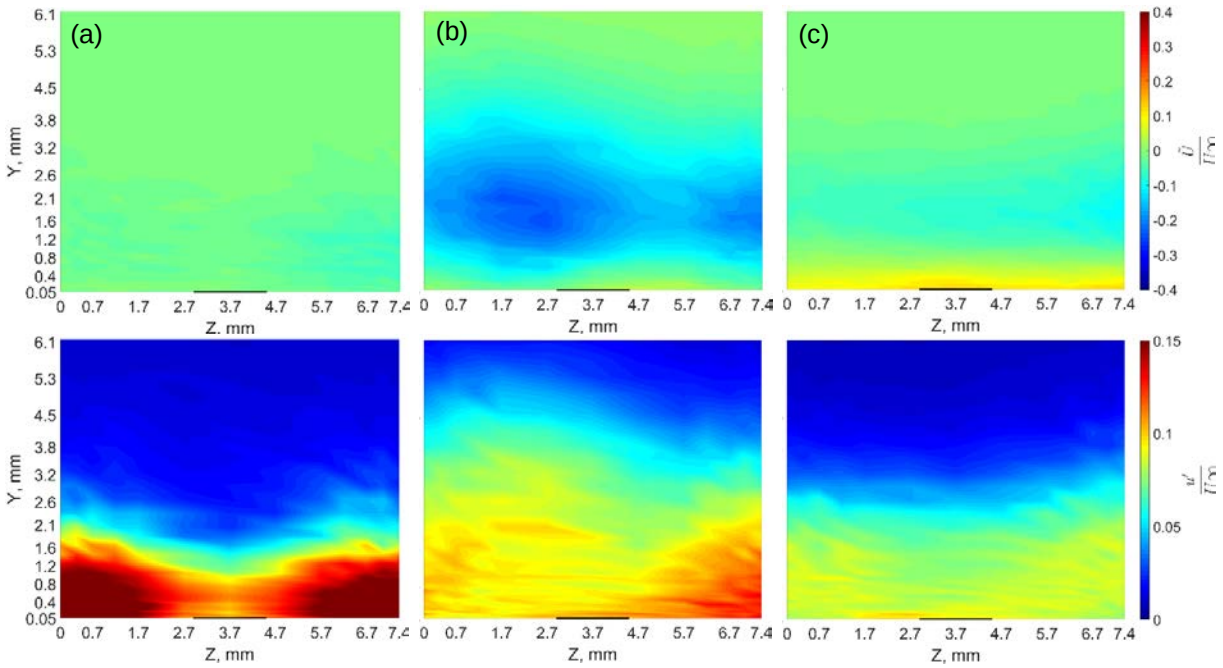

Fig. 11 Velocity perturbation (top row) and rms velocity fluctuation (bottom row) contours in y-z plane on a serrated trailing edge at (a) t = 4.8 ms, (b) t = 11.6 ms and (c) t = 19 ms; measured at $x_s/2h = 0.8$

Further development of the calm region is demonstrated in Fig. 12. At t = 22.8ms the calm region gains more strength and, interestingly, at the same time seems to begin breaking up into several separate regions. Separation between them gradually increases with time until we see two separate regions with reduced magnitude of perturbations. As the calm region undergoes these structural changes, the high turbulence intensity region gets gradually more suppressed until it leaves no traces at t = 30.6ms. However, the plot at t = 40.2ms shows that the high momentum regions regain some of the strength and then eventually dissipates again at t = 46ms. After this instance, the regions of concentrated momentum appear for several more occasions with gradually decreasing magnitude until eventually the flow returns to the state that we observed prior to arrival the spot. Similarly, the high turbulence intensity regions eventually return to their initial state as the calm region passes.

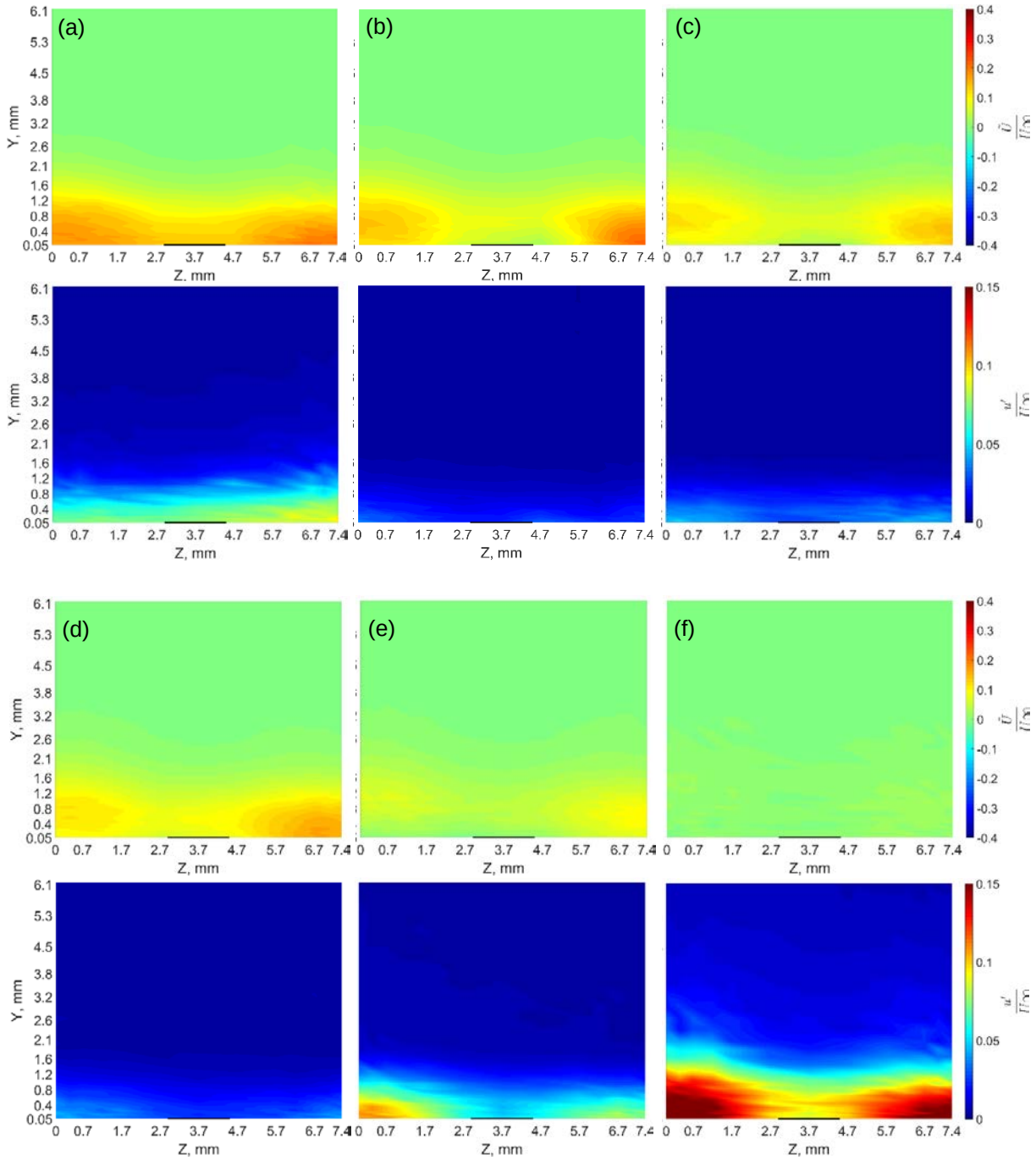

Fig. 12 Velocity perturbation (top row) and rms velocity fluctuation (bottom row) contours in y-z plane on a serrated trailing edge at (a) t = 22.8 ms, (b) t = 30.6 ms, (c) t = 36.2 ms, (d) t = 40.2 ms, (e) t = 46 ms and (f) t = 59.6 ms; measured at xs/2h = 0.8

3. Turbulent spot in x-z plane

The previously described results are expanded on in this section by analyzing results obtained by taking measurements in the X-Z plane (refer to Fig. 3 for orientation of the plane with respect to the aerofoil trailing edge) located at 0.4mm from the aerofoil, or serration, surface. Since the previously presented results have already indicated that changes only appear to occur in within the calm region of the turbulent spot, it will mostly be the point of focus when analyzing the flow measurements in this plane.

Viewing the previously observed (see Fig. 11a) high turbulence intensity region form the top (see Fig. 13a) we can clearly see that with the exception of serration tip, it almost entirely misses the serration surface, confirming the previous speculation that the origin of the high level velocity fluctuations is the serration roots.

Even at an early stage of turbulent spot arrival, Fig. 13b, the high momentum flow demonstrates the tendency to seep into the empty spaces between serrations and this is in agreement with findings reported in [13]. As the spot progresses, the flow with higher magnitude perturbations continues to 'fill' the root regions until it is almost entirely confined within them at t = 40ms.

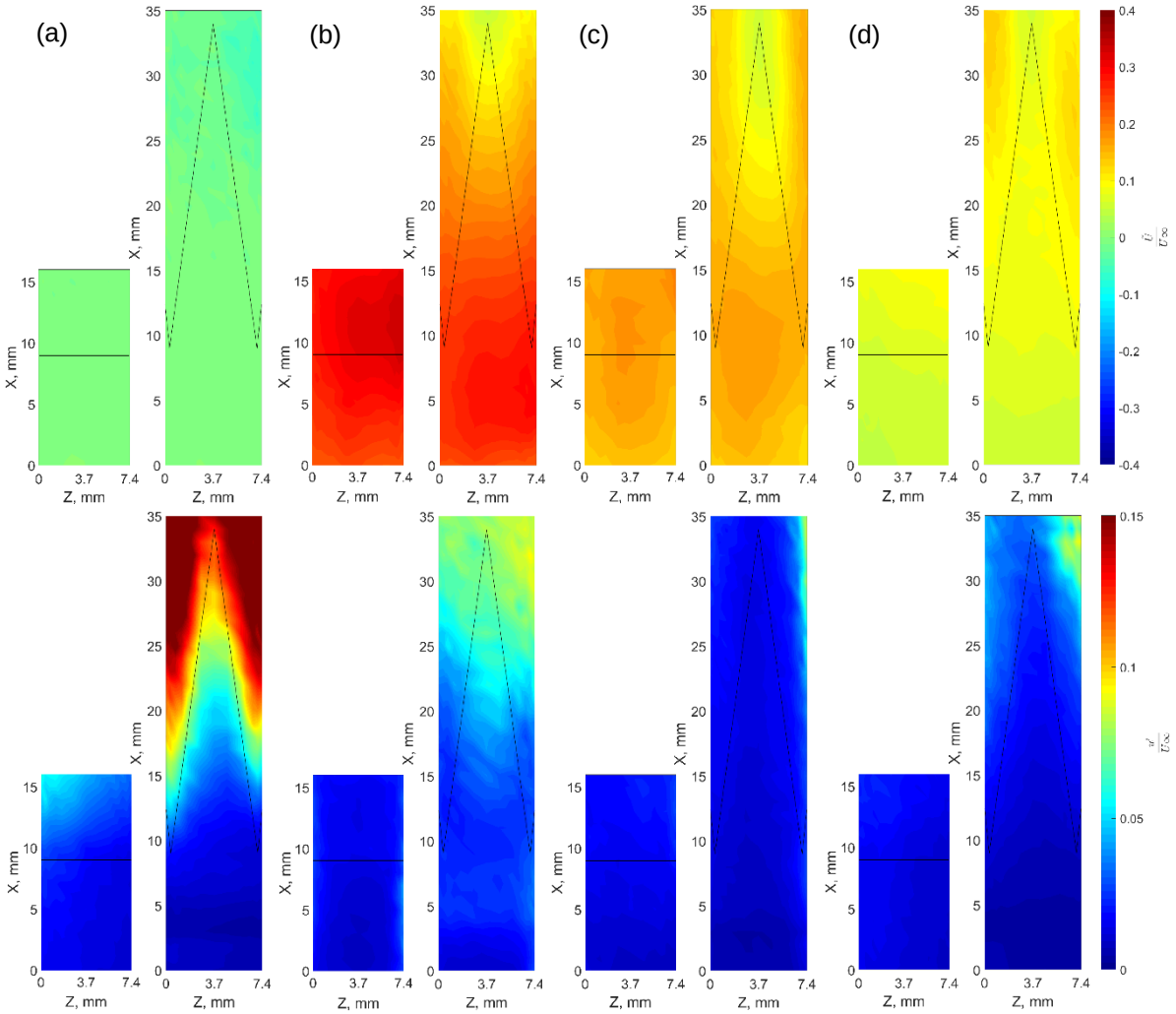

Fig. 13 Velocity perturbation (top row) and rms velocity fluctuation (bottom row) contours in x-z plane on a baseline and serrated trailing edges at (a) t = 4.8 ms, (b) t = 23 ms, (c) t = 29.4 ms and (d) t = 40 ms; measured at y = 0.4mm

4. Turbulent spot in y-z plane in the wake region

All of the results presented prior to this section have only focused on the u velocity component. Cross-wire measurements in the near wake region (1 mm from the straight trailing edge for the baseline case and 1 mm from the serration tip for the serrated trailing edge case) are following the same patters already observed in the previous sections in terms of the u velocity component. This is apparent in Fig. 14a and Fig. 14b, where at t = 25.6ms we see the existence of a uniformly distributed calm region in the baseline trailing edge case and regions of concentrated high momentum flow in the serration roots in the serrated trailing edge case. Note that this and other figures presented in this section do not take into account the time delay that is present due to the two measurement planes (for baseline and serrated trailing edge cases) being 25mm apart. Similarity of the results is also apparent from the velocity fluctuation contours presented in Fig. 14a and Fig. 14b, where at t = 4.8ms baseline case demonstrates only minor fluctuations whereas serrated trailing edge case shows regions of high turbulence intensity flow, similarly to that

demonstrated in Fig. 11a. For this reason, majority of the focus in this section will be drawn towards the results of the w velocity component data.

Another useful observation from the results presented in Fig. 14 is that upper and lower sides demonstrate structures that are reasonably symmetric, indicating that the spots generated on both upper and lower sides of the aerofoil are similar.

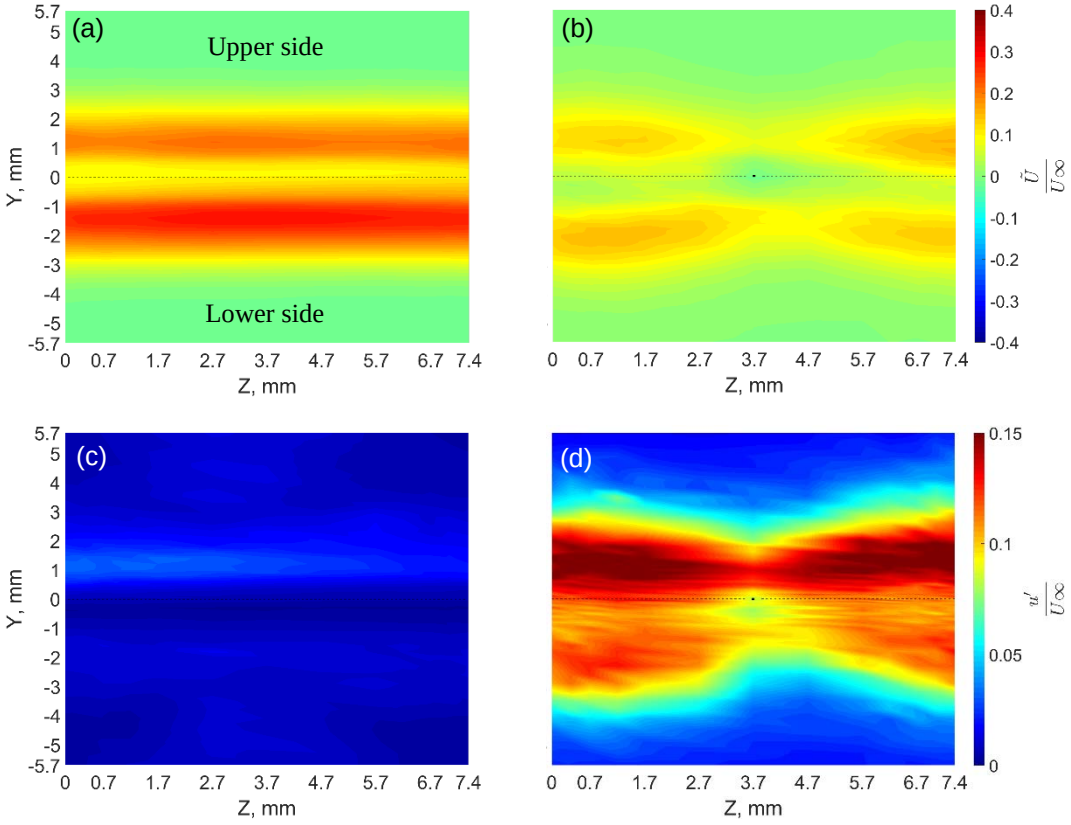

Fig. 14 Velocity perturbation, (a) and (b), and rms velocity fluctuation, (c) and (d), contours of u velocity component caused by the passage of an ensemble averaged turbulent spot across a Y-Z plane measured at 1mm in the aerofoil wake; baseline (left) and serrated (right) trailing edges; dashed line indicates the vertical location of the trailing edge, solid dot indicates the serration tip

Initially, while the laminar flow is still present before arrival of the turbulent spot, contrary to the baseline trailing edge case, high turbulence intensity region (see Fig. 15) around the serration tip is present. This, combined with the observation of high turbulence intensity regions of the u component in the serration roots, might be an indication that even without the presence of fully established turbulent flow, serrations are already inducing oblique vortices originating at the serration roots that would tend to reside around the serration edges. This would partially explain the high turbulence intensity of the u component in the serration roots, as shown in Fig. 11a, Fig. 13a and Fig. 14d (note that all three figures present the flow state at the same time instance) as well as the high rms velocity fluctuations of the w component. Presence of such flow regime with vortical flow motion around the tip would therefore result in a region of spanwise fluctuations of the w component (as shown in Fig. 15) that we observe.

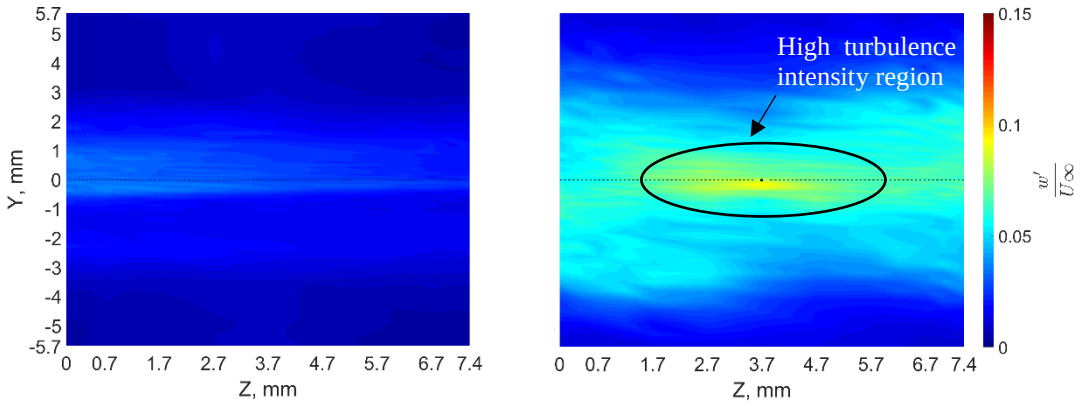

Fig. 15 Rms velocity fluctuation contours of w velocity component caused by the passage of an ensemble averaged turbulent spot across a Y-Z plane measured at 1mm in the aerofoil wake; baseline (left) and serrated (right) trailing edges; t = 4.8ms

However, the interaction between serrations and the passage of the turbulent spot seems to be inducing changes to the structure of the turbulent spot (as it has been shown in earlier sections and will be shown) independently of the phenomenon described in the previous paragraph. This might be an indicator that the processes that are underwent by an isolated turbulent spot could also be occurring when trailing edge serrations interact with a fully established turbulent boundary layer.

As mentioned earlier, the most significant changes are observed in the calm region of the turbulent spot. Arrival and passage of the calm region is not as apparent from the contours of w component, therefore perturbations of u component are used as a reference to the location within the calm region of the spot. Fig. 16 demonstrates that at t = 33ms the turbulent spot is at the stage where the calm region is already displaying the previously observed (see Fig. 12a) regions of high momentum flow coinciding with the serration roots. At the same time instant, rms velocity fluctuation contour is indicating two regions of noticeably (about 6%) increased turbulence intensity that also coincide with the root regions. As mentioned earlier, the phenomenon where high momentum flow is drawn into the serration root regions occurs periodically. Such periodic occurrence also seems to apply to the fluctuations in the w component that appear to be varying in magnitude with time. Interestingly, both of these processes, the drawing of high momentum flow in the u component and the spanwise fluctuations in the w component, are occurring at a similar frequency, meaning that they are interlinked. Moreover, the fact that this structure, caused by fluctuations of the w component, resembles no similarity to the structure that is observed prior to the spot's arrival (see 'High turbulence intensity region' in Fig. 15) might show that their behaviour is not affected by each other's presence. However, this cannot be established until the data are more conclusive.

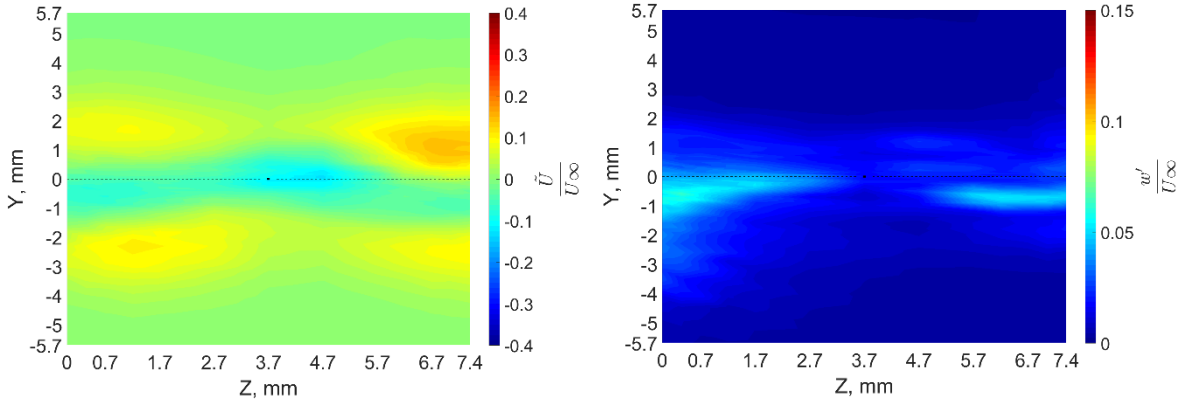

Fig. 16 Velocity perturbation contours of u velocity component (left) and rms velocity fluctuation contours of w velocity component (right) caused by the passage of an ensemble averaged turbulent spot across a Y-Z plane measured at 1mm in the aerofoil wake; baseline (left) and serrated (right) trailing edges; both contours are presented at the same time instance of t = 33ms

IV. Conclusion

This paper has presented experimental results of the flow measurements on a symmetric NACA 0008 aerofoil subjected to flat-plate insert-type trailing edge serrations. More specifically, it is attempted to describe the temporal-spatial development of artificially generated turbulent spots as they pass through a baseline and serrated trailing edges. The main outcomes of the investigation are therefore as follows:

1. It is identified that in presence of laminar flow, or prior to arrival of the turbulent spot, serrations induce a secondary flow mechanism that manifests itself as a significantly increased regions of turbulence intensity. It seems to originate from the serration root region and tend to completely avoid any interaction with the serration surface.
2. High turbulence intensity reigons described in 1. are completely suppressed upon arrival of the turbulent spot, mainly due to high stability of the calm region of the spot. This result might have implications on transitional noise where, similarly to the current experimental setup, part of the flow is laminar and turbulent spots are appearing randomly and intermittently. This observation will form part of the future studies.
3. Serrations induce significant changes to the structure of the turbulent spot, and this mostly occurs within the serration root region. Interestingly, most of the changes seem to be confined within the so called 'calm region' of the spot which is known to possess high stability. This gives rise to a hypothesis that the flow regime that causes these flow disruptions must possess high strength, higher than that of the 'calm region'.

Despite of the experimental observations made within this paper, little connection is provided to the aero-acoustic performance aspect of trailing edge serrations. Therefore, the study will shift focus to bridge the gap between the current study and the reductions of radiated noise that have been demonstrated in this paper. This will be achieved by employing the wavelet analysis technique to describe the temporal change of noise spectrum produced by an artificially generated turbulent boundary layer as it passess though the trailing edge serrations.

The presented flow measurements also have significant limitations considering that only the streamwise velocity component is measured in most cases, hence it is planned to include cross-wire (to provide data of the u and v velocity components) as well as Particle Image Velocimetry measurements in future studies to provide more indepth look into the flow phenomena that have been observed so far.

Acknowledgments

The authors would like to thank for the financial support from the EPSRC Doctoral Training Partnership (DTP), and the EPSRC Research Grant No: EP/N018737/1 on the "Quiet Aerofoils of the Next Generation".

References

[1] A. Nghiem, I. Pineda, and P. Tardieu, "Wind energy in Europe: Scenarios for 2030," 2017.

[2] T. F. Brooks, S. Pope, and M. A. Marcolini, "Airfoil Self-Noise and Prediction," *NASA Ref. Publ. 1218*, pp. 1–142, 1989.

[3] S. Oerlemans, M. Fisher, T. Maeder, and K. Kögler, "Reduction of Wind Turbine Noise Using Optimized Airfoils and Trailing-Edge Serrations," *AIAA Journal*, vol. 47, no. 6, pp. 1470–1481, 2009.

[4] K. Braun *et al.*, "Serrated trailing edge noise (STENO)," Proceeding of the European Union Wind Energy Conference and Exhibition., pp. 180–183, 1999.

[5] T. P. Chong and P. F. Joseph, "An experimental study of airfoil instability tonal noise with trailing edge serrations," *Journal of Sound and Vibration*, vol. 332, no. 24, pp. 6335–6358, 2013.

[6] T. P. Chong, A. Vathylakis, P. Joseph, and M. Gruber, "On the Noise and Wake flow of an Airfoil with Broken and Serrated Trailing Edges," 17th *AIAA/CEAS Aeroacoustics Conference, AIAA 2011-2860*, Portland, USA, 2011.

[7] T. Dassen, R. Parchen, J. Bruggeman, and F. Hagg, "Results of a wind tunnel study on the reduction of airfoil self-noise by the application of serrated blade trailing edges," Proceeding of the European Union Wind Energy Conference and Exhibition, September, pp. 800–803, 1996.

[8] M. Gruber, M. Azarpeyvand, and P. F. Joseph, "Airfoil trailing edge noise reduction by the introduction of sawtooth and slitted trailing edge geometries," *Proc. 20th Int. Congr. Acoust. ICA*, vol. 10, no. August, pp. 1–9, 2010.

[9] M. S. Howe, "Noise produced by a sawtooth trailing edge," *J. Acoust. Soc. Am.*, vol. 90, no. 1, pp. 482–487, 1991.

[10] M. Gruber, P. Joseph, and T. P. Chong, "Experimental Investigation of Airfoil Self Noise and Turbulent Wake Reduction by the use of Trailing Edge Serrations," *16th AIAA/CEAS Aeroacoustics Conference.*, AIAA 2010-

3803, Stockhold, Sweden, 2010.
[11] T. P. Chong and A. Vathylakis, "On the aeroacoustic and flow structures developed on a flat plate with a serrated sawtooth trailing edge," *Journal of Sound and Vibration.*, vol. 354, pp. 65–90, 2015.
[12] M. Gruber, "Airfoil noise reduction by edge treatments by Mathieu Gruber Thesis for the degree of Doctor of Philosophy," 2012.
[13] F. Avallone, S. Pröbsting, and D. Ragni, "Three-dimensional flow field over a trailing-edge serration and implications on broadband noise," *Physics of Fluids*, vol. 28, no. 11, 2016.
[14] W. C. van der Velden, F. Avallone, and D. Ragni, "Numerical analysis of noise reduction mechanisms of serrated trailing edges under zero lift condition," *23rd AIAA/CEAS Aeroacoustic conference*, AIAA-2017-4173, Denver, USA, 2017
[15] R. E. Mayle, "A Theory for Predicting the Turbulent-Spot Production Rate," *Journal of Turbomachinery*, vol. 121, no. July, p. 588, 1999.
[16] G. B. Schubauer and P. S. Klebanoff, "Contributions on the mechanics of boundary-layer transition," *NACA Technical Report 1289*, vol. NACA-TR-12. p. 93R21575, 1955.
[17] C. Y. Ching and J. E. LaGraff, "Measurement of turbulent spot convection rates in a transitional boundary layer," *Exp. Therm. Fluid Sci.*, vol. 11, no. 1, pp. 52–60, 1995.
[18] I. Wygnanski, M. Sokolov, and D. Friedman, "On a turbulent 'spot' in a laminar boundary layer," *Journal of Fluid Mechanics*, vol. 78, no. 4, pp. 785–819, 1976.
[19] A. E. Perry, T. T. Lim, and E. W. Teh, "A visual study of turbulent spots," *Journal of Fluid Mechanics*, vol. 104, no. 1, p. 387, 1981.
[20] M. Gad-El-Hak, R. F. Blackwelderf, and J. J. Riley, "On the growth of turbulent regions in laminar boundary layers,"*Journal of Flui Mechanics*, vol. 110, pp. 73–95, 1981.
[21] J. H. Vathylakis, A., Chong, T.P., Kim, "Design of a low-noise aeroacoustic wind tunnel facility at Brunel University," in *20th AIAA/CEAS Aeroacoustics Conference*, AIAA-2014-3288, Atlanta, USA, 2014
[22] J. P. Gostelow, N. Melwani, and G. J. Walker, "Effects of Streamwise Pressure Gradient on Turbulent Spot Development," *Journal of Turbomachinery*, vol. 118, no. 4, pp. 737–743, 1996.